HMS developments for the rocket engine demonstrator Mascotte

A. Iannetti[1] and S. Palerm[2]
CNES Launcher Department, Paris, France

J. Marzat[3], H. Piet-Lahanier[4] and G. Ordonneau[5]
ONERA-The French Aerospace Lab, Palaiseau, France

This paper summarises the latest HMS developments for the cryogenic test bench MASCOTTE. Cnes and Onera have worked together to build an HMS benchmark demonstrator with the aim of testing new monitoring approaches for a cryogenic rocket engine representative system such as MASCOTTE. The work performed, the algorithms developed and the results obtained so far are presented in this paper.

Nomenclature

P_1 = pressure in cavity 1 (Pa)
P_2 = pressure in cavity 2 (Pa)
k_p = pressure drop coefficient (non dimensional)
ρ = water density (kg/m^3)
a = speed of sound in water (m/s)
c_v = specific heat of water at constant volume (J/(kg.K))
V_1 = volume of cavity 1 (m^3)
V_2 = volume of cavity 2 (m^3)
S = cross sectional area for the orifice element (m^2)
$q = q_1^s = q_2^e$ = mass flow through the orifice element, at cavity 1outlet and at inlet of cavity 2 (kg/s)
q_1^e = cavity 1 inlet mass flow (kg/s)
q_2^s = cavity 2 outlet mass flow (kg/s)
T_1 = temperature in cavity 1 (K)
T_2 = temperature in cavity 2 (K)
$\dot{Q}_1$ = heat flux on cavity 1 (W)
$\dot{Q}_2$ = heat flux on cavity 2 (W)
μ = dynamic viscosity (kg/(s.m))
D_h = characteristic dimension cross flow, hydraulic diameter (m)
L = characteristic length of the flow (m)
h_{water} = convective coefficient (W/K/m^2
k_{wall} = wall heat conductivity (W/K/m
Δx = conduction length (m)
$S_{exchange}$ = surface for the heat exchange between the heated wall and water cooling volume of cavity 2 (m^2)

---

[1] Liquid Propulsion System Specialist, CNES Launcher Technical Division, 52 rue J. Hillairet, Paris 75012, France
[2] R&T Liquid Propulsion Manager, CNES launcher directorate, 52 rue J. Hillairet, Paris 75012, France
[3] Research Engineer, ONERA – The French Aerospace Lab, F-91123 Palaiseau, France
[4] Senior Research engineer, ONERA – The French Aerospace Lab, F-91123 Palaiseau, France
[5] Head of Liquid Propulsion Unit, ONERA Fundamental and Applied Energetics Department, 29 av. de la Division Leclerc, Châtillon 92290, France

T_{wall} = temperature at the cooled surface water side (K)

I. Introduction

DURING the last decades, several research efforts have been conducted to improve the diagnosis methods of rocket engines for applications at test bench or during flight. Current monitoring strategies rely mostly on redline systems which are simple to set but are sources of human errors and rely on sensors availability. The possible control strategies are also limited as the detection latency of redlines can be large in order to avoid high false alarm rates. The latest diagnosis technics together with the new computational power available on board and at test benches provide a potential to optimize engine exploitation. Besides flight application, for test bench application, real time predictive monitoring can reduce the risk of hardware failure, the time of operations at bench in case of anomalous shut-down, and finally speed up data exploitation and analysis.

The results of this work is the development of a diagnostic benchmark for the cryogenic test bench Mascotte.

Starting from academic diagnosis methods, we developed a diagnosis strategy that we tested on data from past firing tests. We analysed the diagnosis performances with multiple combinations of failure modes thanks to a functional benchmark. The aim of the work is to improve the real time monitoring of the bench Mascotte to contribute to demonstration of methodologies and strategies of HMS for liquid rocket engines.

II. Background

With focus on improving existing rocket engine systems for future competitive launchers, CNES has worked in the area of health monitoring technics since many years, [1,15-17] . In the last two years in particular a new research cooperation was put into place with Onera and provided the opportunity to couple three main HMS competence domains: algorithmics and diagnosis from ONERA data treatement and diagnosis department,[9,10,11,18,19,20] , propulsion experimental skills from Onera Propulsion division,[4,21] and the rocket engine system expertise from CNES liquid propulsion team. As a matter of fact the two entities were also cooperating in studies on cryogenic combustion for more than 10 years within the project Mascotte, [4], and the latest test experiences at the bench in Palaiseau showed the potential for improvement of the real time monitoring strategy. Mascotte becomes thus the natural environment to demonstrate new HMS technics and to grow expertise for the cryogenic propulsion application.

The operational experience from the Mascotte team was the basis for the diagnostic benchmark development: the risk analysis, the sensors characteristics and the functional aspects are the starting point for our HMS developments.

III. Mascotte cryogenic test bench

MASCOTTE test bench was designed to study cryogenic rocket combustion and nozzle flow performances. It was built in 1994 from the cooperation between CNES and ONERA, [4]. Several versions of the hardware of both bench and combustors were developed during the years for different purposes. The most recent version of combustor called ATAC-HRM is used to analyze rocket nozzle performances at high mixture ratio[22]. The combustion chamber fed with gaseous hydrogen and oxygen is terminated by a 2D nozzle. All the hardware has been equipped with a water cooling circuit in order to withstand high mixture ratio and pressure in the chamber and to run longer duration (up to 150s). Figure 1 shows the chamber section and the bi-dimensional nozzle. The overall water circuit of the bench is shown in Fig. 2.

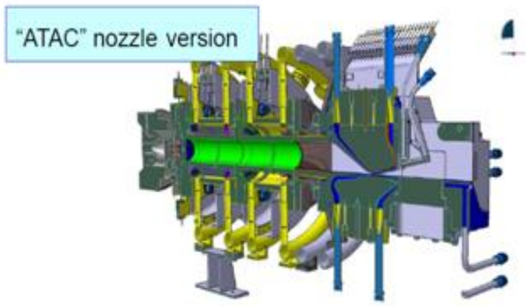

Figure 1. Combustion and nozzle. *Yellow section with water cooling system (yellow parts).*

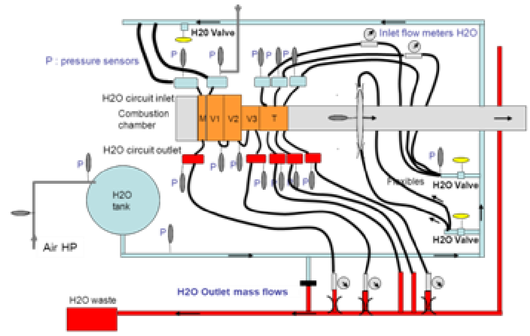

Figure 2. Test bench water cooling circuit. *M = inlet chamber section, V1 to V3 = middle chamber sections, T = nozzle.*

The bench is monitored and controlled via three main computers. Fig. 3 shows the front end of the bench, and Fig. 4 is an example of the graphic interface used to set the redlines. The diagnosis system is currently based on independent redlines on relevant parameters. These ones are selected as risk reduction solutions associated to the potential hazards of the test campaign. The detailed risk analysis is performed before each test campaign and all redlines are agreed by the campaign responsibles. The choices performed are dictated by experience, bench control capabilities and test campaign objectives. In the frame of this work we selected one particular critical subsystem of the bench, namelythe water circuit. This one allows the cooling of the different combustion chamber sections and of the bidimensional nozzle,enabling longer combustion duration and higher mixture ratio. Redlines of the water circuit are set for pressures, mass flows and temperatures. Minimum and maximum allowable values are set manually in the control computer; each redline is independent. The bench controller works in open loop mode and so a test stop is issued whenever one or more of the monitored parameters cross the set redlines for more than a minimum time.

In such an experimental set up, experience had shown the difficulty in the choice of the thresholds when testing new hardware designs, and also the limited knowledge available in real time does not permit efficient decision making in case of unexpected events that would still allow continuation of the testing.

Figure 3. Bench control. *Control computers and bench front end electronics at MASCOTTE test bench premises at Onera (Palaiseau, France).*

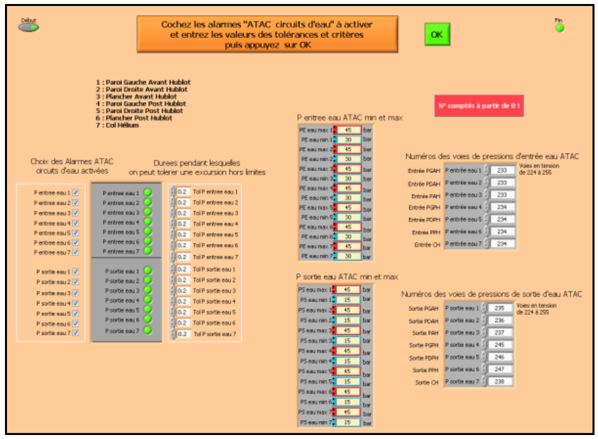

Figure 4. Redlines graphic interface. *Example of interface for the manual set up of redlines (Labview environment).*

IV. Fault diagnosis methods

Model-based fault detection methods are one of the most common diagnostic technics used in process monitoring for a wide range of applications (ex. nuclear, aeronautics, chemical etc.) [2,3,5,6]. A mathematical model represents the knowledge of the process and it is used to produce diagnosis flags based on deviations of parameters from their nominal expected values. These deviations (residuals) can be obtained from the evaluation of characteristic parameters of the system as in parameter estimation methods [5] or directly from sensor output estimations as in Kalman filtering approaches [6]. Finally statistical tests on the residuals are performed to obtain robust diagnosis flags (i.e. CUSUM test [9]).

Among the many model-based methods available we selected a least-square parameter identification and a Kalman filter approach. We performed an analysis of the possible modelling of the cooling system and a simplified model was put into place describing the main processes in each branch of the water circuit. This model is the basis of our diagnosis strategy.

V. Water cooling system model

The chamber or nozzle section in Fig. 1 is modelled through an inlet cavity, an orifice and an outlet cavity. Fig. 5 shows the corresponding zones. "Cavity 1" corresponds to the inlet volume of the cooling circuit, "Orifice" is the connecting tube ensuring the mass flow and "Cavity 2" the water volume flowing on the chamber wall and heated up by the combustion process. This scheme can be applied to any other segment of the water circuit: the three chamber segments (V1 and V2, V3 in Fig. 2) and the bi-dimensional nozzle part (T in Fig. 2).

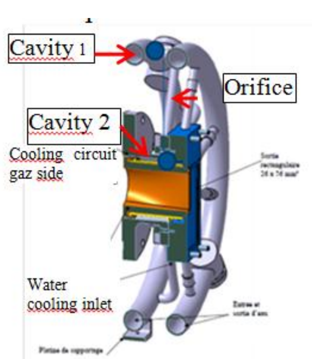

Figure 5. Cavities and orifices modelling. *Cavity and orifice principle applied to a generic water system sections*

This modelling approach is directly inspired by the CNES software CARMEN [7] which is used for modelling rocket engine systems. It was extensively validated on different engines and propulsive systems. The idea here is to build a simple and generic model applicable to different system parts. The dynamical equations from conservation laws applied to each element are written and they constitute the model base for the algorithm development.

Cavity 1:

$$\frac{dP_1}{dt} = (q_1^e - q_1^s) \cdot \frac{a^2}{V_1}$$
$$\frac{dT_1}{dt} = \frac{1}{\rho \cdot V_1} \cdot (q_1^e T_1^e - q_1^s T_1) + \frac{\dot{Q}_1}{c_v \rho V_1} \qquad (1)$$

Liquid orifice:

$$P_1 - P_2 = \frac{k_p}{\rho S^2} \cdot q^2$$
$$q = \sqrt{\frac{P_1 - P_2}{k_p} \cdot \rho S^2} \qquad (2)$$

Cavity 2:

$$\frac{dP_2}{dt} = (q_2^e - q_2^s) \cdot \frac{a^2}{V_2}$$
$$\frac{dT_2}{dt} = \frac{1}{\rho \cdot V_2} \cdot \left(q_2^e T_2^e - q_2^s T_2\right) + \frac{\dot{Q}_2}{c_v \rho V_2} \qquad (3)$$

Let us consider first Eq. (1), (2) for establishing a model of pressure and mass flow evolution. Assuming $q_1^s = q_2^e$ the resulting equation for each branch of the circuit is Eq. (4) below.

$$\frac{dP_2}{dt} = \left(\sqrt{\frac{P_1 - P_2}{k_p} \cdot \rho S^2} - q_2^s\right) \cdot \frac{a^2}{V_2} \qquad (4)$$

Introducing the parameter $M = 0.3164 \cdot \left(\frac{1}{\frac{\pi D_h}{4} \cdot \mu}\right)^{-0.25} \cdot \frac{L}{D_h} \cdot \frac{1}{2}$ and the derivative of state variable $\dot{P}_2 = \frac{dP_2}{dt}$ in Eq. (4), we obtain Eq. (7). Complete details of the model development can be found in Ref. 8.

$$\dot{P}_2 = \frac{a^2}{V_2} \cdot \left(-q_2(t) + q_2^{0.125}(t) \cdot \sqrt{\frac{\rho \cdot S^2}{M}} \cdot \sqrt{P_1(t) - P_2(t)}\right) \qquad (5)$$

With additional constant parameters $b = \frac{a^2}{V}$, $c = \left(\frac{\rho \cdot S^2}{M}\right)^{\frac{1}{2}}$, the final model is expressed in Eq. (6).

$$\dot{P}_2 = b \cdot \left(-q_2(t) + c \cdot q_2^{0.125}(t) \cdot \sqrt{P_1(t) - P_2(t)}\right) \qquad (6)$$

Introducing a simple expression for the heat flux through the water circuit in Eq. (5) and a global heat exchange coefficient as in Eq. (6):

$$\dot{Q}_2 = h_{water} \cdot \left(\frac{1}{1 + h_{water} \cdot \frac{\Delta x}{k_{wall}}}\right) \cdot (T_{wall} - T_2) \cdot S_{exchange} \qquad (7)$$

$$H = h_{water} \cdot \left(\frac{1}{1 + h_{water} \cdot \frac{\Delta x}{k_{wall}}} \right) \cdot \frac{S_{exchange}}{c_v \cdot \rho \cdot V_2} \tag{8}$$

We obtain a simplified equation for the thermal equation of cavity 2 as in Eq. (6).

$$\frac{dT_2}{dt} = \frac{1}{\rho \cdot V_2} \cdot q_2 (T_2^e - T_2) + H \cdot (T_{wall} - T_2) \tag{9}$$

These expressions are the basis of the development of the predictive monitoring strategies tested in the frame of this work.

VI. Model-based diagnosis tools development and validation

Based on the mathematical model described above, we developed two approaches: parameter identification and Kalman filter for the hydraulic behaviour (pressure and mass flows monitoring), [8]; a Kalman filter for the diagnosis of the thermal behavior, [12]. The CUSUM test is used to analyze the diagnostic residuals,[9]. The algorithms were tested over different firing campaign results and have given good results for the monitoring of the hydraulic and thermal behaviour of the water circuit. Detailed description of the algorithms can be found in Ref. 8 and 12. A synthesis of the results obtained is provided in section A. and B..

A. Parameter identification method

This technic allows to identify a characteristic parameter, here named ‘c’, of the water circuit assumed to be constant for different testing campaign and to be self tuned. The parameter value calculation is based on geometry and thermophysical data of the circuit and its online value is identified on the basis of pressure and massflow measurement.

For steady state behaviour a recursive least-square identification algorithm is employed for estimating the value of the parameter ‘*c’* based on the measurements of q_2 , P_1 and P_2. Equation (6), for steady state phase can be written under the form $y = h \cdot c$ where $y = q_2(t)$ and $h = q_2^{0.125}(t) \cdot \sqrt{P_1(t) - P_2(t)}$.

The parameter is initialized with $c(0) = c_0$, where c_0 can be an a priori guess or it can be automatically identified on a nominal firing interval, and the parameter variance $v(0) = v_0$. The update at each time step is then performed recursively by minimizing the expression $\|Y_N - H_N\|_2^2$ where Y_N and H_N are the sequences of *y* and *h* from time 0 to *N*.

The a priori guess of the paramer was validated through test data and it was also proved that it was constant using results of different years of testing campaigns and for different combustion or nozzle sections (a maximum variance of 10% was found). This technics could not be employed for the thermal behaviour as no characteristic constant parameter could be found.

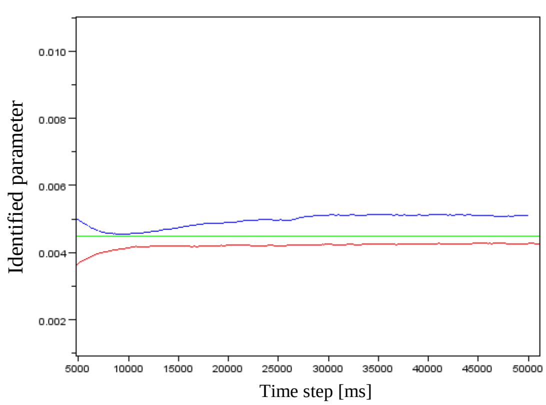

Figure 6. Chamber part identification. Characteristic parameter estimation for different testing campaigns

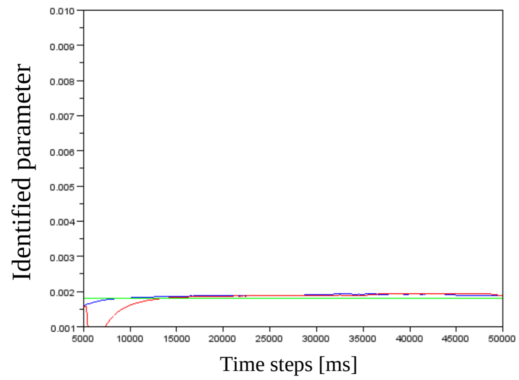

Figure 7. Nozzle part identification. Characteristic parameter estimation for different testing campaigns.

The algorithm provides a generic and automatic approach for steady state monitoring. At each time step the update value of the parameter is compared to the reference one and any deviation from nominal steady state behaviour is identified in real time. Compared to redlines, this also allows to check consistency of different measurements and it gives an overall estimation of the functional behaviour of the water circuit hydraulics.

B. Kalman filter method

Two Kalman filters were developed respectively for the hydraulic and thermal behaviour monitoring. They can be used for detection in steady state but also for smooth transient phases.

Based on the simplified model equations an extended Kalman filter was used. The state and input noise varianceswere based on the sensors noises. For the hydraulic monitoring the outlet pressure from cavity 2 was reconstituted based on massflow and inlet pressure. The dynamic equations for the filter development are based on Eq. (5) plus simplified dynamics for constant parameters in Eq. (5). The final system is given in Eq. 10 and it shows that the estimated value of the pressure is based on other measurement inputs. In case of sensor malfunction a pressure estimate could still be provided by the algorithm. For diagnosis purpose any abnormal deviation from the nominal expected behavior is identified by comparison of the estimated value with the pressure measurement.

$$\begin{aligned} \dot{P}_2 &= -bq_2\,(t) + d \cdot q_2^{0.125}(t) \cdot \sqrt{P_1(t) - P_2(t)} \\ \dot{d} &= 0 \end{aligned} \tag{10}$$

For the thermal behaviour monitoring, the state space system is given in Eq. (11).

$$\begin{aligned} \frac{dT_2}{dt} &= \frac{1}{\rho \cdot V_2} \cdot q_2(T_2^e - T_2) + H \cdot (T_{wall} - T_2) \\ \frac{dH}{dt} &= 0 \end{aligned} \tag{11}$$

As it is shown from Fig. 8 and 9, the filters converge quickly and provide good estimation of pressure or temperature for different firing campaigns with different objectifs. The estimations integrate sensor noise and do not depend on the many specific operating points of the test campaign.

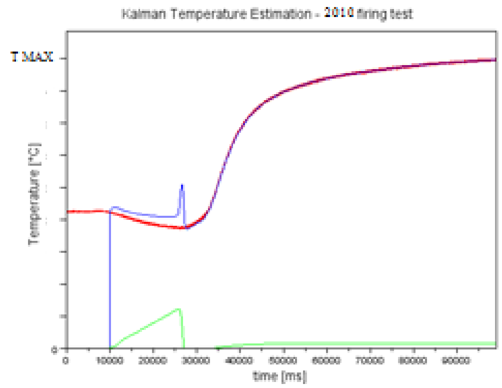

Figure 8. Thermal Kalman prediction. *Combustion chamber section, RED = temperature measurement, BLUE = Kalman estimation, GREEN = estimated H parameter. Validation on firing tests data from 2010.*

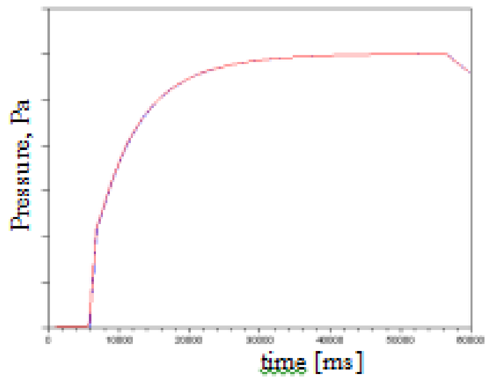

Figure 9. Pressure Kalman prediction. *Combustion chamber section RED = temperature measurement, BLUE = Kalman estimation, GREEN = estimated H parameter. Validation on firing tests data from 2014.*

C. Residual analysis for detection flag

Thanks to the monitoring tools developed, we are able to provide a prediction of specific measurement or characteristic parameter of the water circuit. To obtain a diagnosis flag it is necessary to compare the prediction with the measurement or the identified parameter. This is performed with a CUSUM test approach, a very common test to detect changes in data, where no statistical hypothesis are necessary,[9,13,14] .

Equations (12) give the expression of the CUSUM sums.

$$\begin{aligned} S_1(t) &= \max\left(S_1(t-1) + r(t) - \mu_0 - \delta, 0\right) \\ S_2(t) &= \max\left(S_2(t-1) - r(t) + \mu_0 - \delta, 0\right) \end{aligned} \tag{12}$$

The parameter δ is the minimal size of the faulty variation to be detected. The decision rule is if ($S1 > \lambda\,\delta$) or ($S2 > \lambda\,\delta$) decide fault, else decide no fault. The parameter λ is a user threshold, r(t) is the residual and μ_0 is the residual average. The value of threshold λ has an impact on the detection delay and for the chosen application it helps reduce signal noise false alarm.

VII. Diagnostic benchmark

Once the HMS tools were available and validated, the need was to create an environment to quantitatively analyse their diagnostic performances to prepare the integration in the bench environment. In order to analyse different failure scenarios, a functional simulator of the bench was build with the software CARINS. This allowed us to test the algorithms over different functional combinations on pressure, mass flow and temperature but also different intensities and failure rates. Sensor noise was also included on the simulated output.

Two main diagnosis performance parameters were considered such as the good detection rate and the false alarm rate. For more detailed description, see [12]Ref 12.

D. Mascotte Carins simulator

The main elements of the simulator are: gaseous Oxygen (GOX) and gaseous hydrogen (GH2) feed lines, igniter line, combustion chamber, water system circuit for the chamber and nozzle (ATAC).

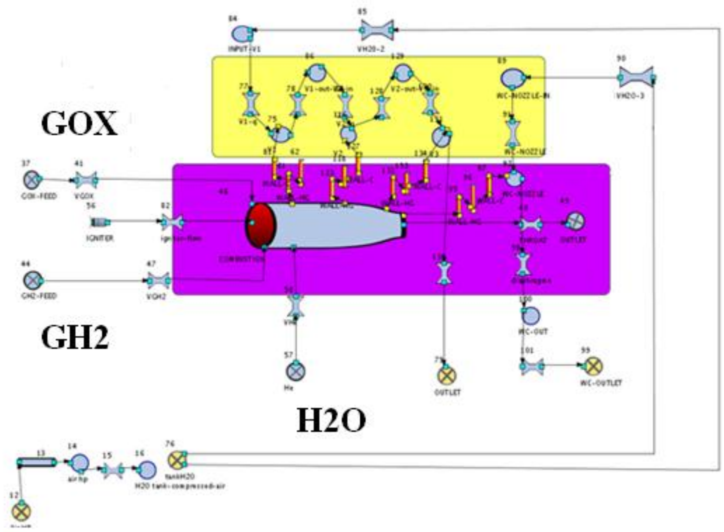

Figure 10. CARINS simulator of the Mascotte test bench. *Purple zone is for the combustion chamber, yellow zone represents the water circuit.*

The simulator was validated over nominal data from firing tests, it gives a good representation of the dynamic behaviour of the bench. For the steady-state part, we found maximum errors of 10% and for the transient phases maximum errors of 7%.

E. Failure case descritpion

Three types of failures were modelled with the CARINS simulator:

- L1: Hydrogen feeding valve partial obstruction (section reduction) with an indirect impact on the water circuit wall temperature due to a sudden increase of the combustion temperature (no impact on pressure and mass flow in the water circuit);
- L2: obstruction in the outlet orifice of the water circuit combustion section (V2 in Figure 2) with a direct impact on all water circuit measurements;
- L3: leakage from cavity 1 of V2 (a mass flow is diverted from the main flow of the inlet cavity), direct impact on all water circuit measurements.

Each failure scenario is simulated with different failure ratios and intensities as shown in Fig. 11. A typical failure is a quick failure with a transient phase of 10 ms while the B-type is slower with a transient phase of 2 s. These transients are representative of fast and slow failure modes for rocket engines. The intensities of the failure that is the valve obstruction or the diverted leakage, are 10%, 30% and 50% of the nominal value. These are referred to as low, mid and max failure levels.

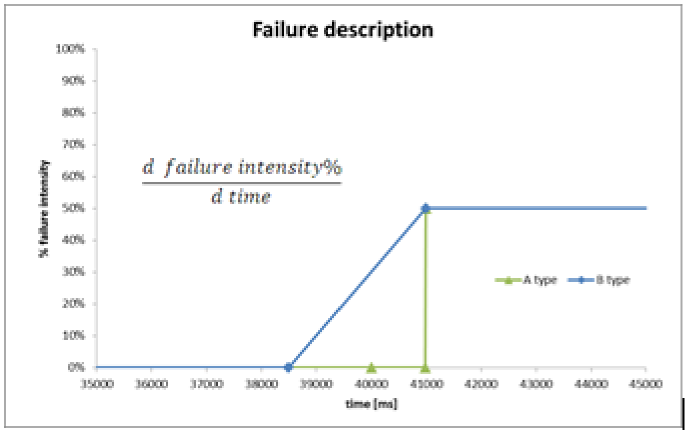

Figure 11. Failure description. *Two different failure rates were tested, A type and B type. Different intensities were used.*

F. Diagnosis performances analysis

We calculated the good detection and the false detection rates over a time interval of 10s in a steady-state phase. During this interval the injected failure is persistent (as shown in Fig. 11). The good detection rate is the ratio in % of the time, the flag is raised while the failure is present and the duration of the failure; the false detection is the ratio in % of time a detection flag is raised during the time interval of nominal operation.

The choice of the detection parameter for each algorithm is function of the sensor noise. This is straightforward for the Kalman filters as they directly estimate one sensed parameter but it is more difficult for parameter identification algorithm as the identified parameter has a nonlinear (square root) dependency on the measured variables. To reduce noise sensitivy on the CUSUM test we used λ =2.

As presented in Ref. 12, results obtained with varying CUSUM settings and for the different failure scenarios, at maximum intensity, show very good detection rate for parameter identification algorithm between 90 and 98%. False alarme rate is around 1%. Detection performances do not decrease for slower transient types. For the Kalman filter, detection performance for quick failures is slightly better than for parameter identification but it fails to detect slower failure rate. False alarms are always less than 1%. The best choice of detection limit for the CUSUM test for both methods corresponds to the noise standard deviation. Both methods also provide good isolation capability of hydraulic versus thermal failure types as they do not detect anything for L1 failure case (only impact on temperatures). The results for the Kalman thermal algorithm show good performances for abrupt failure types such as A-types, while for B-types good detection was possible only for the most intense L1 failure (25% increase on the temperature). More analysis could be performed on the Kalman filter settings to improve this behaviour.

A quick overview of the algorithms scores is provided in Table 1 for failure scenario L3.

Table 1. Sensibility to fault intensity and rate

Failure intensity (leak %)	max		mid		low	
fault transient type	Quick	Slow	Quick	Slow	Quick	Slow
Parameter Identification. gd %	99.2	91.3	98.76	88.6	61	45.9
Parameter Identification. fd %	1.4	1.4	1.41	0.96	1.34	1.2
Kalman Presure. gd%	99.3	97.6	99.27	85.54	99.27	0.95
Kalman Pressure. fd%	0.02	0.06	0.03	0.02	0.03	0.0
Kalman Temperature gd%	96.2	0.03	78.54	0	0.01	0
Kalman Temperature. fd%	0.02	0.0	0.02	0.02	0.02	0.01

VIII. Conclusions

Thanks to a successful cooperation between CNES and ONERA a new environment for HMS expertise was put into place. This environment based on multidisciplinary competences covering all the critical aspects linked to HMS such as diagnostics, propulsion modeling, test bench experience, allowed to build and test a custom methodology for HMS development and analysis.

The quantitative analysis performed with the benchmark showed that simple classical model based diagnosis approaches can be applied to a rocket system. A generic diagnosis setup could be identified providing good detection rates for different failure types, intensities and rates. This confirms the interest of the diagnosis approach compared to the basic redlines, which have to be set depending on the specific test configuration (e.g. target operating pressures) and the specific failure types to monitor.

Future work includes improvement of the algorithms, integration in the Mascotte bench control environment and test in real time.

References

[1] Iannetti, A., (2014). *Overview on European efforts on health monitoring/management systems for rocket engines*. Space Propulsion Conference, Köln, Germany.

[2] Ding, S.X., (2008), *Model-based fault diagnosis techniques*, Springer Verlag, Berlin Heidelberg.

[3] Blanke, M., Kinnaert, M., Lunze, J., Staroswiecki, M., (2003). *Diagnosis and Fault-Tolerant Control*. Springer Verlag, Berlin Heidelberg

[4] Ordonneau, G., Hervat, P., Vingert, L., Petitot, S., Pouffary, B., (2013). *First results of heat transfer measurements in a new water-cooled combustor on the Mascotte facility.* 4th European conference for aerospace sciences (EUCASS).

[5] Isermann, R., (1984). *Process fault detection based on modeling and estimation methods—a survey.* Automatica, Vol. 20(4), pages 387-404.

[6] Chow, E., Willsky, A.S., (1984). *Analytical redundancy and the design of robust failure detection systems.* IEEE Transactions on Automatic Control, Vol. 29(7), pages 603-614.

[7] Cliquet, E., Iannetti, A., Masse, J., (2009). *Carmen, liquid propulsion systems simulation platform.* European conference for aerospace sciences (EUCASS).

[8] Iannetti, A., Marzat, J., Piet-Lahanier, H. et al., (2014), *Development of model based fault diagnosis algorithms for the Mascotte cryogenic test bench.* IOP Journal of Physics: Conference Series, ACD Berlin.

[9] Marzat, J., Walter, E., Piet-Lahanier, H., Damongeot, F., (2010). *Automatic tuning via kriging-based optimization of methods for fault detection and isolation.* IEEE Conference on control and fault tolerant systems, Nice, France, pages 505-510.

[10] Marzat J., Piet-Lahanier H., Damongeot F., Walter E., *Control-based fault detection and isolation for autonomous aircraft,* Proceedings of the IMechE, Part G : Journal of Aerospace Engineering, 226(5), 2012 - Available online http://pig.sagepub.com/content/early/2011/11/08/0954410011413834

[11] Marzat J., Piet-Lahanier H., Damongeot F., Walter E., *Model-based fault diagnosis for aerospace systems: a survey*, Proceedings of the IMechE, Part G :Journal of Aerospace Engineering, 226(10), 2012 - Available online http://pig.sagepub.com/content/early/2012/01/06/0954410011421717

[12] Iannetti A., Marzat J., Piet-Lahanier H., Ordonneau G., Vingert L., *Fault diagnosis benchmark for a rocket engine demonstrator,* 9th IFAC Symposium on Fault Detection, Supervision and Safety for Technical Processes, Paris, France, September 2-4, 2015

[13] M. Basseville, I. V. Nikiforov, *Detection of Abrupt Changes: Theory and Application.* Prentice Hall Englewood Cliffs, NJ, 1993.

[14] F. Gustafsson, *Adaptive Filtering and Change Detection*. Wiley London, 2001

[15] S. Benoit, P. Bornert, S. Legonidec, P. Supié, *"A diagnostic demonstrator: a platform for the evaluation of real time diagnostic data dedicated to space engines",* MFPT2009

[16] A. Iannetti, G. Ramusat et al. *"Structural Health Monitoring for European reusable Launch Vehicles", Third European Workshop on Structural health Monitoring*, 5-7 July 2006

[17] T. Kachler et al. *"Liquid Propulsion technology maturation in the frame of the FLPP main stage propulsion project*", Eucass 2012

[18] M. Balesdent, H. Piet-Lahanier, *"A multi-level Optimization approach for the planning of heterogeneous sensor network*", Modeling, Computation and optimization in information systems and management sciences, pages 221-233, Springer International Publishing, ISBN 978-3-319-18166-0

[19] J. Marzat, H. Piet-Lahanier, F. Damongeot, E. Walter, *"Tuning and comparing fault diagnosis methods for aeronautical systems via kriging-based optimization",* Eucass proceedings Series 12/2013

[20] S. Bertrand, J. Marzat, H. Piet-Lahanier, A. Kahn, Y Rochefort, *"MPC Strategies for cooperative guidance of autonomous vehicles",* Aerial Robotics, AerospaceLab journal, Issue 8 December 2014

[21] R.G. Stutzer, J. Sender, N. Fdida, L. Vingert, G. Ordonneau, A. Ristori, *„Characterisation of a double swirl injector in a LOX/LCH4 fueled combustor on Mascotte test bench",* EUCASS 2013

[22] G. Ordonneau, F. Grisch, L. Vingert, P. Hervat, P Reijasse "*PLIF Investigation of Reactive Flows in the Separation Region of an Over-Expanded Two-Dimensional Nozzle*", 42nd AIAA/ASME/SAE/ASEE Joint Propulsion Conference & Exhibit, Sacramento (2006). (http://arc.aiaa.org/doi/abs/10.2514/6.2006-5209)